NASA MEMO 1-31-59L

NASA

MEMORANDUM

PARASITE-DRAG MEASUREMENTS OF

FIVE HELICOPTER ROTOR HUBS

By Gary B. Churchill and Robert D. Harrington

Langley Research Center
Langley Field, Va.

NATIONAL AERONAUTICS AND
SPACE ADMINISTRATION

WASHINGTON

February 1959

NATIONAL AERONAUTICS AND SPACE ADMINISTRATION

MEMORANDUM 1-31-59L

PARASITE-DRAG MEASUREMENTS OF FIVE HELICOPTER ROTOR HUBS

By Gary B. Churchill and Robert D. Harrington

SUMMARY

An investigation has been conducted in the Langley full-scale tunnel to determine the parasite drag of five production-type helicopter rotor hubs. Some simple fairing arrangements were attempted in an effort to reduce the hub drag.

The results indicate that, within the range of the tests, changes in angle of attack, hub rotational speed, and forward speed generally had only a small effect on the equivalent flat-plate area representing parasite drag. The drag coefficients of the basic hubs, based on projected hub frontal area, increased with hub area and varied from 0.5 to 0.76 for the hubs tested.

INTRODUCTION

It has been shown in reference 1 that the maximum speed and range of a helicopter depend to a large extent on the parasite drag. The parasite drag of such items as landing gears, engine-cooling and exhaust systems, and air leakage through gaps and joints in the structure is well documented and probably requires no further study. The rotor hub, however, is one parasite-drag producing item about which little information is available.

In view of this situation, an experimental investigation has been conducted in the Langley full-scale tunnel to measure the drag of five, representative, production-type rotor hubs mounted on a simple body of revolution. This report presents the results of that investigation. The drag of each hub was measured over an angle-of-attack range from -15° to 5°. Most of the tests were conducted at speeds between 135 and 165 feet per second. In some instances both the hub and control system were tested, while in others the hub alone was tested. In addition to measuring the drag of the basic hubs, some simple fairing arrangements were tested on several of the hubs in an effort to reduce the drag.

SYMBOLS

A_p	projected frontal area of hub, sq ft
C_D	hub parasite-drag coefficient based on projected frontal area, D/qA_p
D	hub parasite drag, lb
D/q	equivalent flat-plate area representing parasite drag, based on unit drag coefficient, sq ft
L/q	equivalent flat-plate area representing lift, based on unit lift coefficient, sq ft
N	rotor-hub rotational speed, rpm
q	dynamic pressure, lb/sq ft
V	velocity, ft/sec
α	angle of attack of hub axis, positive when tilted rearward, deg

APPARATUS AND TESTS

Model

The parasite drag of a helicopter can be influenced to a large extent by the interference drag between the hub and its supporting pylon. (See ref. 2.) Since it was not feasible to duplicate the many possible installations in this investigation, the tests were conducted in such a way as to minimize the effects of interference. A slender, streamlined body (fig. 1) with a 24-inch diameter and fineness ratio of 8 served as a mount for the hubs. Because of its small diameter and high fineness ratio, this body should produce a minimum flow disturbance at the rotor hub over the range of angles of attack of this investigation. Power to turn the rotor hubs was provided by an electric motor driving through a right-angle gear box.

Figure 2 shows the model, with one of the hubs installed, mounted for tests in the Langley full-scale tunnel. The forces and moments on the model were measured on the wind-tunnel balance, a complete description of which is given in reference 3.

Rotor Hubs

The five rotor hubs and the various configurations of each tested in this investigation are shown in figures 3 to 7. Hub 1 (fig. 3) is a direct tilting type. The following configurations were tested:

(1) Basic hub (designated configuration 1A)

(2) Basic hub with simulated blade shanks installed (designated configuration 1B)

(3) Basic hub with blade shanks faired to a fineness ratio of 3 (designated configuration 1C)

Hub 2, which is a teetering type, is shown in figure 4. The control system for this hub was not available for these tests. The following configurations were tested:

(1) Basic hub (designated configuration 2A)

(2) Basic hub with simulated blade shanks installed (designated configuration 2B)

(3) Basic hub with a simple sheet-metal fairing, which would allow the hub to teeter, installed around the blade shanks (designated configuration 2C)

Hub 3, which is also a teetering type, is shown in figure 5. This hub is controlled by a control rotor and swash plate, both of which were available for this investigation. The following configurations were tested:

(1) Basic hub and control system (designated configuration 3A)

(2) Basic hub with simulated blade and control-rotor shanks installed (designated configuration 3B)

(3) Basic hub with control-rotor shanks faired to a fineness ratio of 3 (designated configuration 3C)

(4) Basic hub with a simple sheet-metal fairing, which would allow the hub to teeter, installed around the blade shanks (designated configuration 3D)

Hub 4 (fig. 6) is a fully articulated type and was supplied with a swash plate and control system. The following configurations were tested:

(1) Basic hub and control system (designated configuration 4A)

(2) Basic hub with simulated blade shanks installed (designated configuration 4B)

(3) Basic hub with a trailing-edge fairing added to the blade shanks which effectively extends the rotor-blade airfoil section inboard to the root attachment fitting (designated configuration 4C)

Hub 5, which is also fully articulated, is shown in figure 7. The control system for this hub was not available for these tests. Only two configurations of this hub were tested

(1) Basic hub (designated configuration 5A)

(2) Basic hub with simulated blade shanks installed (designated configuration 5B)

Tests

The forces and moments on the model with each of the hubs installed were measured over an angle-of-attack range from -15° to 5°. Most of the tests were conducted at tunnel speeds from 135 to 165 feet per second.

Since the rotational speed of some of the hubs was limited by vibration (no attempt was made to balance the installations), configuration 1A (fig. 3(a)) was tested over a range of rotational speed to determine the effect of rotational speed on parasite drag. Configuration 4A (fig. 6(a)) was tested over a range of forward speed and angle of attack at constant rotational speed to study the effect of Reynolds number on the parasite drag. The tare drag of the model with no hub installed was measured at each test condition. Drag tares have been subtracted from the data. The test conditions for each hub are given in table I.

RESULTS AND DISCUSSION

Six components of force and moments were measured at each test condition. However, since only the lift and drag of the model varied appreciably with changes in configuration, only the lift and drag components

will be discussed in this report. The tare drag of the model with no hub installed has been removed from all the drag results. No lift tares have been applied.

Effect of Angle of Attack

The variation of the equivalent flat-plate area representing parasite drag D/q with angle of attack for each of the hubs tested is shown in figure 8. In most instances D/q of the basic hubs was relatively constant over the range of α from -15° to 5°. The exception was hub 4 (fig. 8(d), configuration 4A) for which D/q increased from 3.75 square feet at $\alpha = -15^\circ$ to 4.20 square feet at $\alpha = 5^\circ$.

The addition of simulated blade shanks and control-rotor shanks always produced an increase in drag, as would be expected, because of the increase in frontal area. The largest drag increases, on a percentage basis, occurred at $\alpha = -15^\circ$. These increases ranged from 16 percent of the basic-hub drag for hub 2 to 43 percent for hub 4.

Installation of fairings on the hubs, blade shanks, and control-rotor shanks was effective, to various degrees, in reducing the drag of the hubs over most of the angle-of-attack range. However, in one instance the installation of a fairing on the blade shanks of hub 4 (fig. 8(d), configuration 4C) caused an increase in drag at angles of attack below -8°. This might have resulted from an increase in frontal area of the hub at the more negative angles of attack and/or an increase in drag due to lift, as might be inferred from configuration 4C (fig. 9(d)).

The variation of the equivalent flat-plate area representing lift L/q with angle of attack α, for each of the hubs tested, is shown in figure 9. From this figure it can be seen that any modification which adds horizontal area to the hubs, whether it increases or decreases parasite drag, generally causes an increase in the slope of L/q with α. In any analysis to determine the benefits of a fairing, these changes in lift should be accounted for. It should be pointed out again that no lift tares have been removed from these data; therefore, only increments between curves and not the absolute values should be used.

Effect of Rotational Speed and Forward Speed

The effect of changes in rotational speed and forward speed on D/q is shown in figure 10. Changes in rotational speed between 100 and 500 rpm have no effect on D/q and have only a slight effect below 100 rpm. (See fig. 10(a).) The effect of changes in forward speed (fig. 10(b)) is also small, being of the order of 3 percent for speeds

between 80 and 135 feet per second over the angle-of-attack range of the tests. The effects of rotational speed and forward speed shown in figure 10 are in general agreement with the results shown in references 4 and 5 for two different hubs tested in different wind tunnels. It appears that, within reasonable limits, variation in either rotational speed or forward speed will have no significant effect on D/q for any of the hubs. The tests also indicated that effects of rotational speed and forward speed on L/q are of the same order as on D/q and therefore are not included.

Effect of Hub Size

In order to determine the effect of hub size on parasite drag, the D/q values of figure 8 have been reduced to drag coefficients based on the projected frontal area of the basic hubs at $\alpha = 0^{\circ}$. The hub frontal area was determined by integrating the area of a time-exposure photograph of the slowly turning hub. A typical photograph used to determine the projected frontal area of a hub is shown in figure 11. The projected frontal areas of the basic hubs are given in table II. The drag coefficients of the hub configurations tested are shown as a function of angle of attack in figure 12. The variation of C_D with projected frontal area A_p for the basic hubs over the test angle-of-attack range is shown in figure 13. Generally, C_D increases with frontal area; however, this increase is probably due more to aerodynamic uncleanliness of the larger hubs than to Reynolds number effects. Changes in α have no consistent effect on drag coefficient. In these tests, C_D for the basic hubs varied from about 0.5 to 0.76 for the range of hub sizes used in the tests.

CONCLUSIONS

The results of an investigation to measure the parasite drag of five helicopter rotor hubs indicate the following conclusions:

1. In general, angle-of-attack variations did not have large effects on the equivalent flat-plate area representing parasite drag D/q of the basic hubs.

2. Within the limits of these tests, D/q was not significantly affected by changes in hub rotational speed or forward speed.

3. The drag coefficients C_D of the basic hubs, based on projected hub frontal area, increased gradually with hub area and ranged from 0.5 to 0.76 for the hubs tested.

Langley Research Center,
National Aeronautics and Space Administration,
Langley Field, Va., October 20, 1958.

REFERENCES

1. Harrington, Robert D.: Reduction of Helicopter Parasite Drag. NACA TN 3234, 1954.

2. Hickey, David H.: Full-Scale Wind-Tunnel Tests of the Longitudinal Stability and Control Characteristics of the XV-1 Convertiplane in the Autorotating Flight Range. NACA RM A55K21a, 1956.

3. DeFrance, Smith J.: The N.A.C.A. Full-Scale Wind Tunnel. NACA Rep. 459, 1933.

4. Foster, John J.: Wind-Tunnel Tests of a Full-Scale Piasecki H-21 Helicopter Rotor Hub. Rep. 886 Aero Data 8, David Taylor Model Basin, Navy Dept., Aug. 1953.

5. Jones, J. R., and Lund, P. D.: Full Scale Investigation of Rotor Hub Fairing for a Sikorsky H-5 Rotor Hub. Rep. No. 55McC103R (Contract No. AF 18(600)-176), McCulloch Motors Corp., Apr. 1955. (Available from ASTIA as AD No. 93925.)

TABLE I

TEST CONDITIONS FOR ALL HUB CONFIGURATIONS TESTED

Hub configuration	N, rpm	V, ft/sec	α, deg
1A	0, 100, 150, 200	163	-15 to 5
1B	200	163	-15 to 5
1C	200	163	-15 to 5
2A	350	163	-15 to 5
2B	200	163	-15 to 5
2C	200	163	-15 to 5
3A	200	163	-15 to 5
3B	200	163	-15 to 5
3C	200	163	-15 to 5
3D	200	163	-15 to 5
4A	50	79, 95, 115, 137	-15 to 5
4B	50	137	-15 to 5
4C	50	137	-15 to 5
5A	200	137	-15 to 5
5B	200	137	-15 to 5

TABLE II

PROJECTED FRONTAL AREA OF BASIC HUBS

[$\alpha = 0^{\circ}$]

Hub configuration	A_p, sq ft
1A	2.37
2A	1.83
3A	*3.16
4A	*5.36
5A	2.71

*Includes control system.

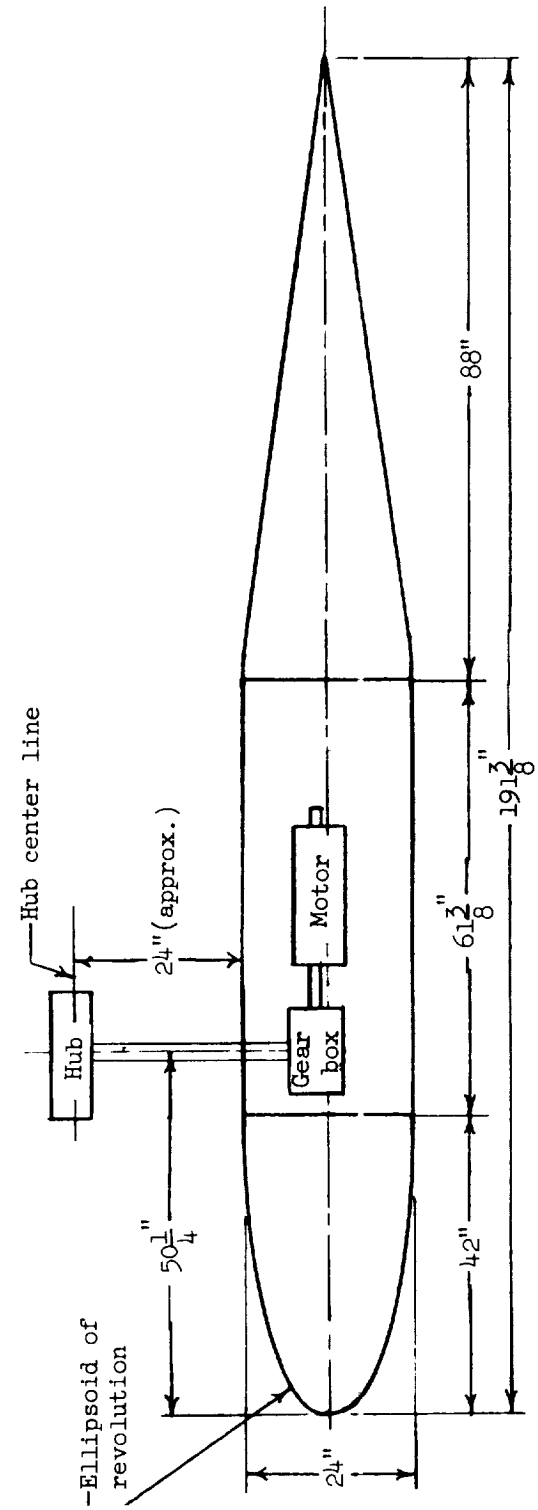

Figure 1.- Sketch of model.

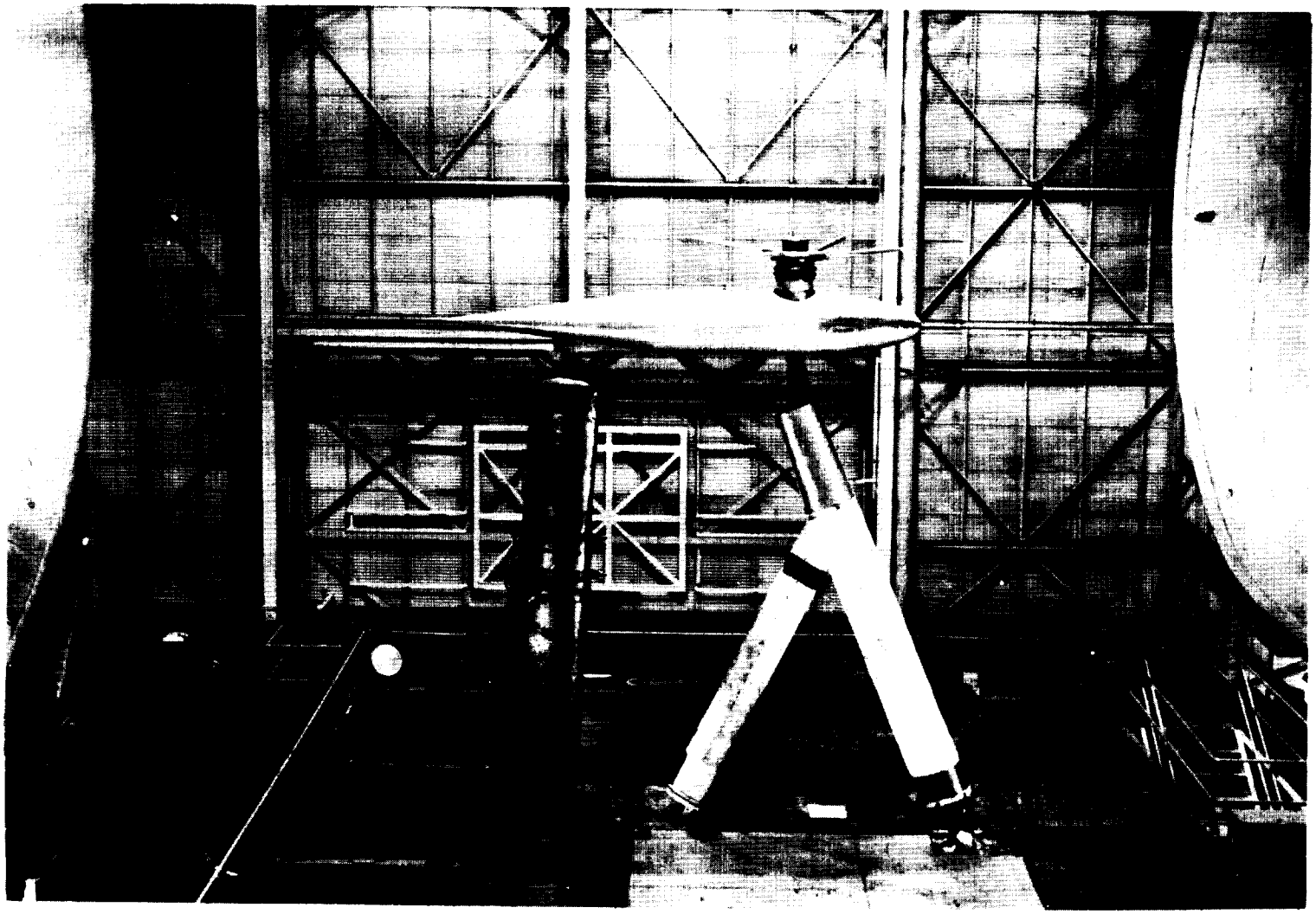

Figure 2.- General view of model in Langley full-scale tunnel. L-89574

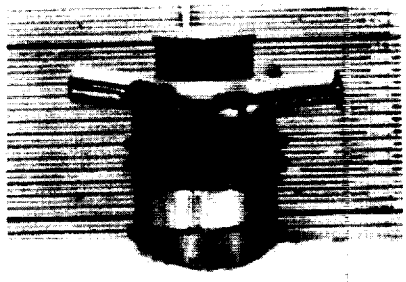

(a) Basic hub (configuration 1A).

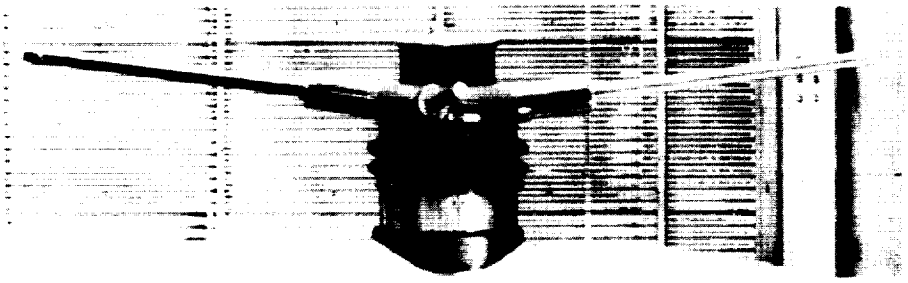

(b) Blade shanks installed (configuration 1B).

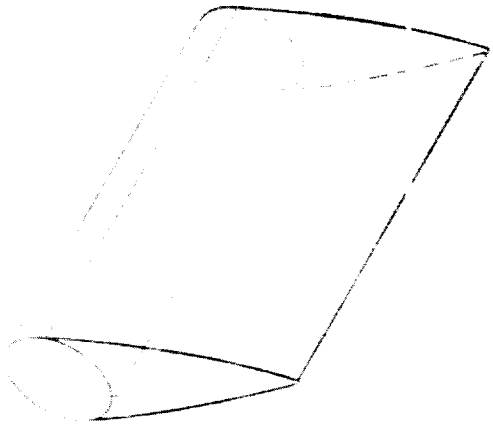

(c) Blade-shank fairing used for configuration 1C. L-58-115a

Figure 3.- Configurations of hub 1.

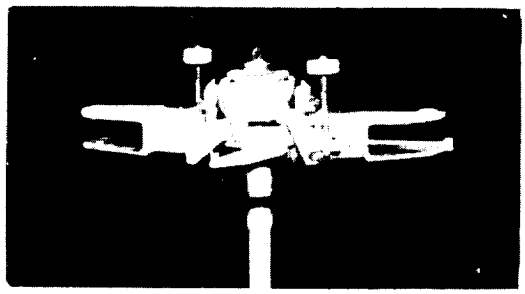

(a) Basic hub (configuration 2A).

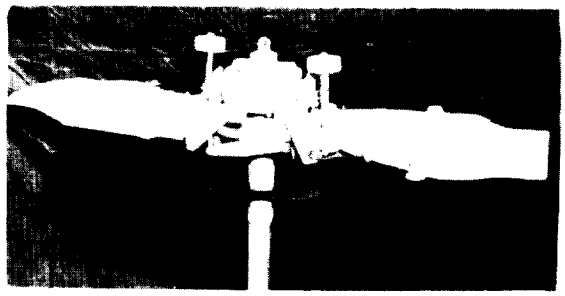

(b) Blade shanks installed (configuration 2B).

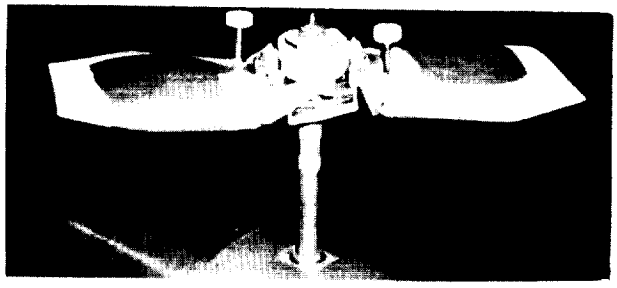

(c) Blade shanks faired (configuration 2C). L-58-116a

Figure 4.- Configurations of hub 2.

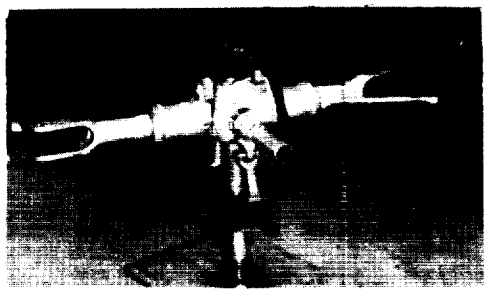

(a) Basic hub and control system (configuration 3A).

(b) Blade shanks and control-rotor shanks installed (configuration 3B).

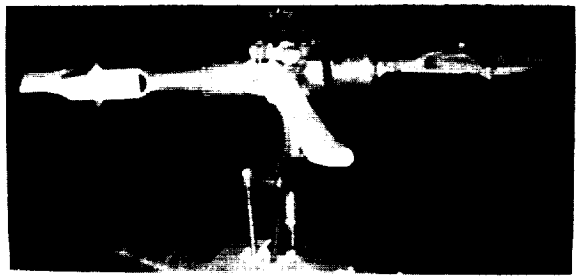

(c) Control-rotor shanks faired (configuration 3C).

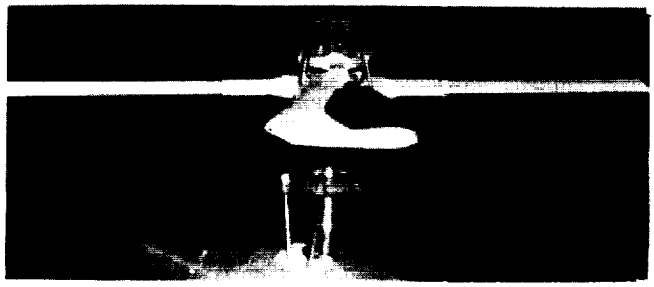

L-58-117a

(d) Blade shanks and control-rotor shanks faired (configuration 3D).

Figure 5.- Configurations of hub 3.

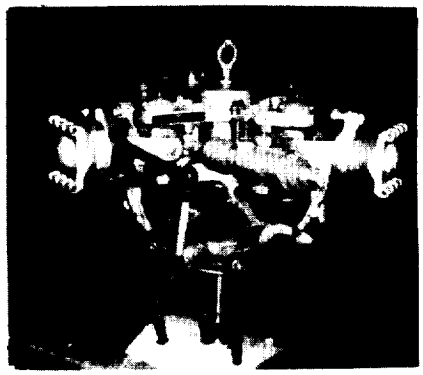

(a) Basic hub and control system (configuration 4A).

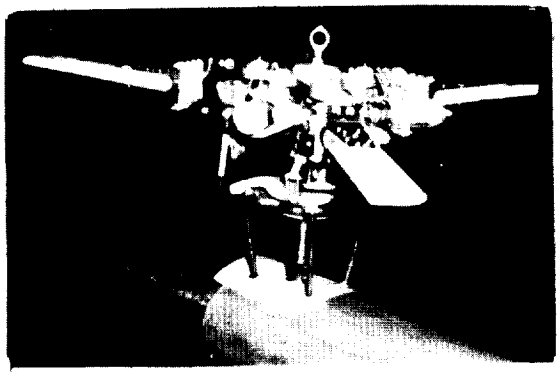

(b) Blade shanks installed (configuration 4B).

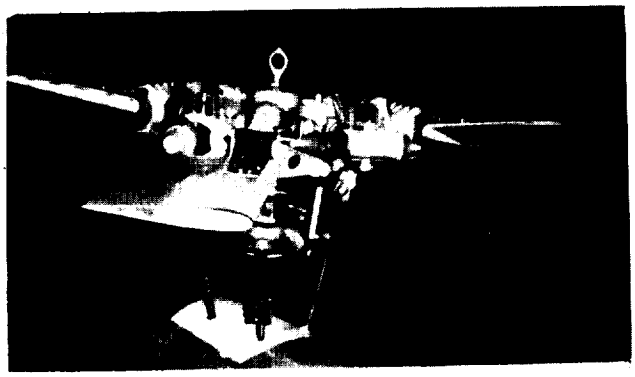

(c) Blade shanks faired (configuration 4C). L-58-118a

Figure 6.- Configurations of hub 4.

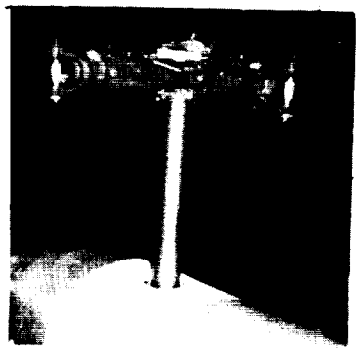

(a) Basic hub (configuration 5A).

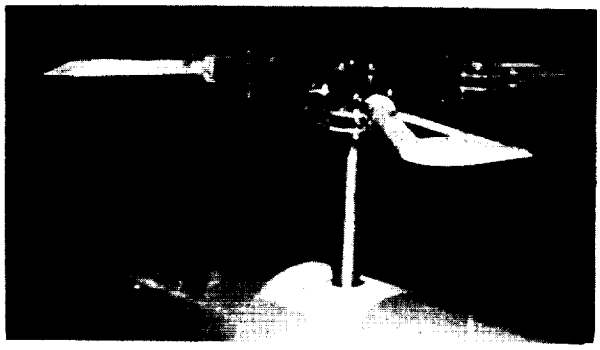

(b) Blade shanks installed (configuration 5B). L-58-119a

Figure 7.- Configurations of hub 5.

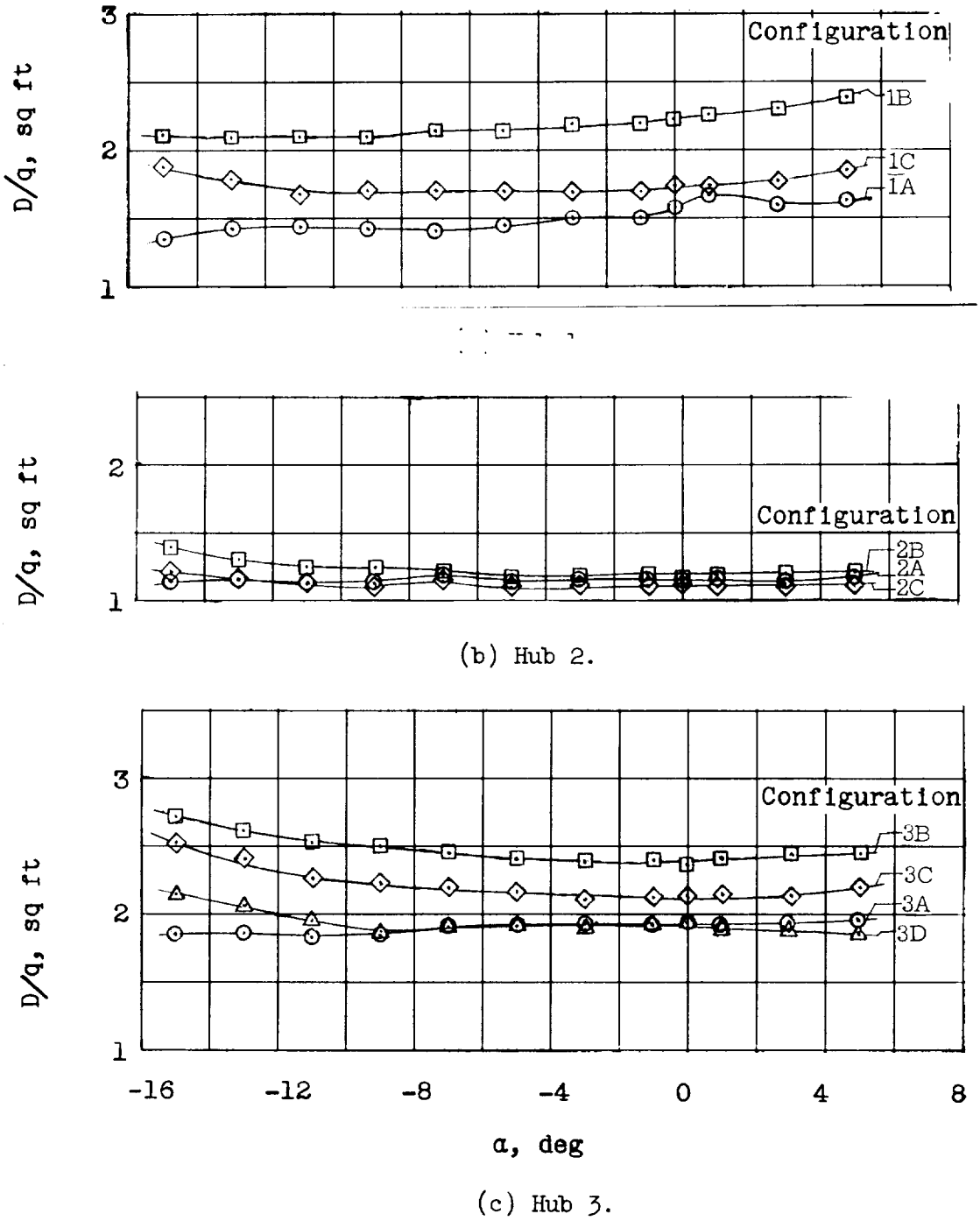

(b) Hub 2.

(c) Hub 3.

Figure 8.- Variation of equivalent flat-plate area representing parasite drag with angle of attack.

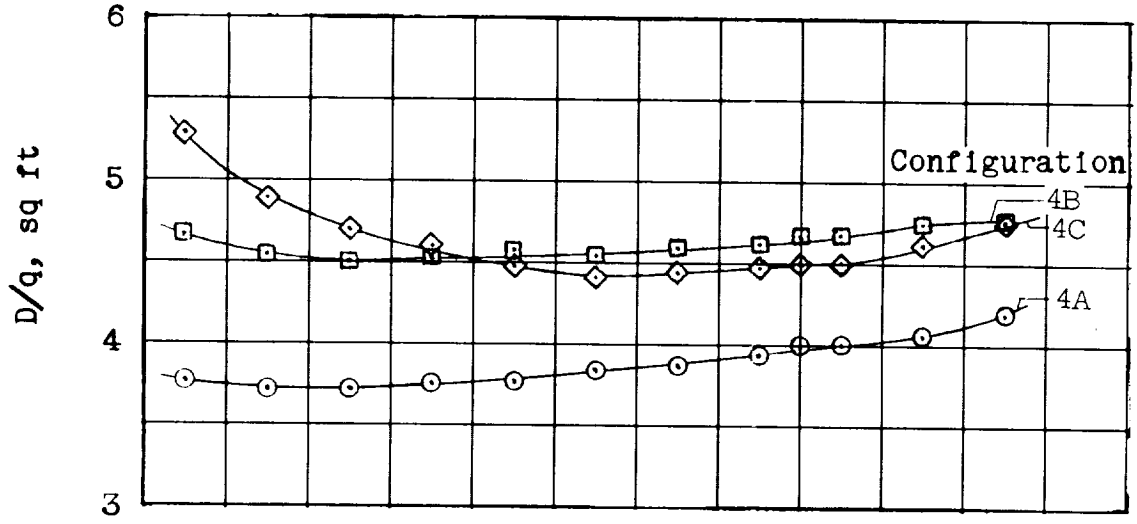

(d) Hub 4.

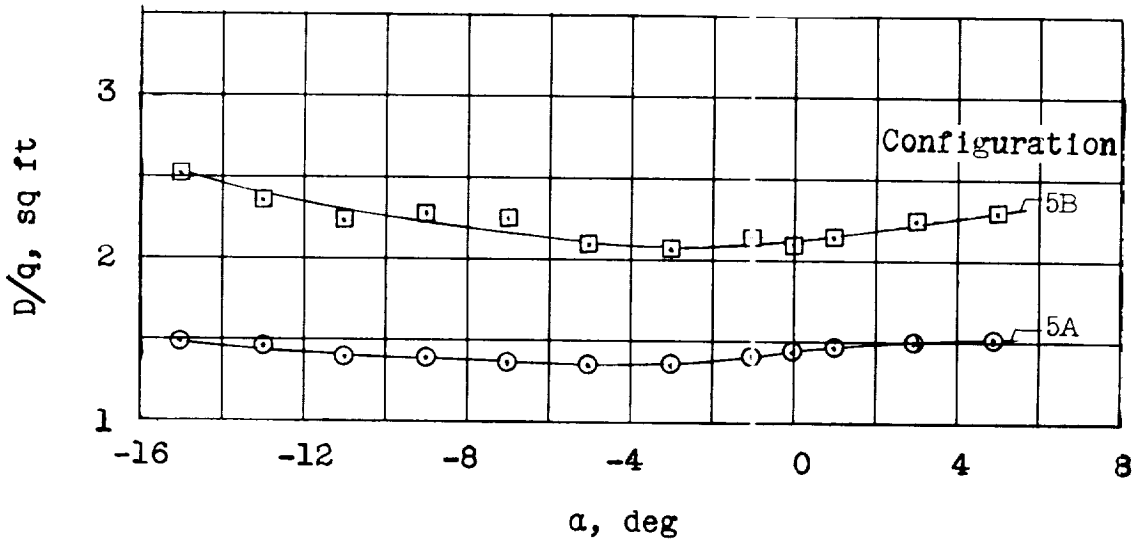

(e) Hub 5.

Figure 8.- Concluded.

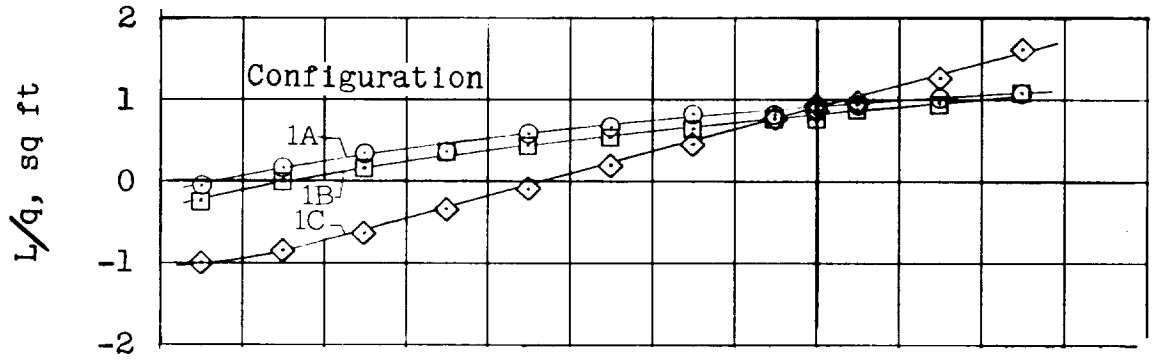

(a) Hub 1.

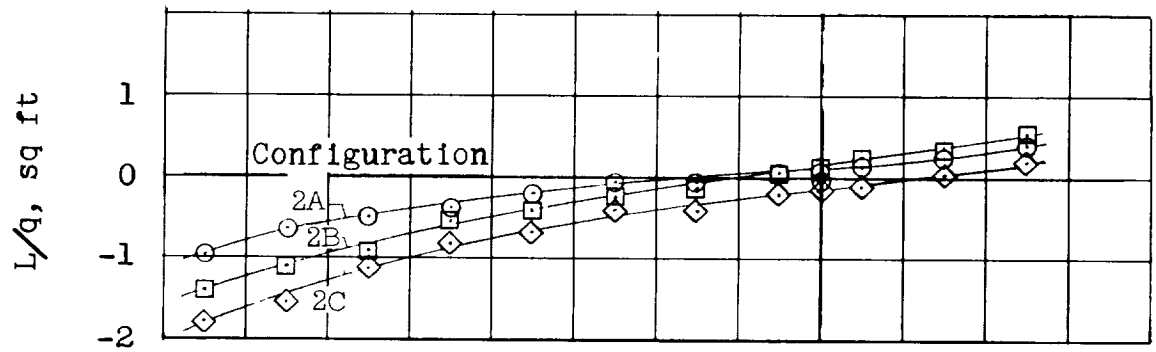

(b) Hub 2.

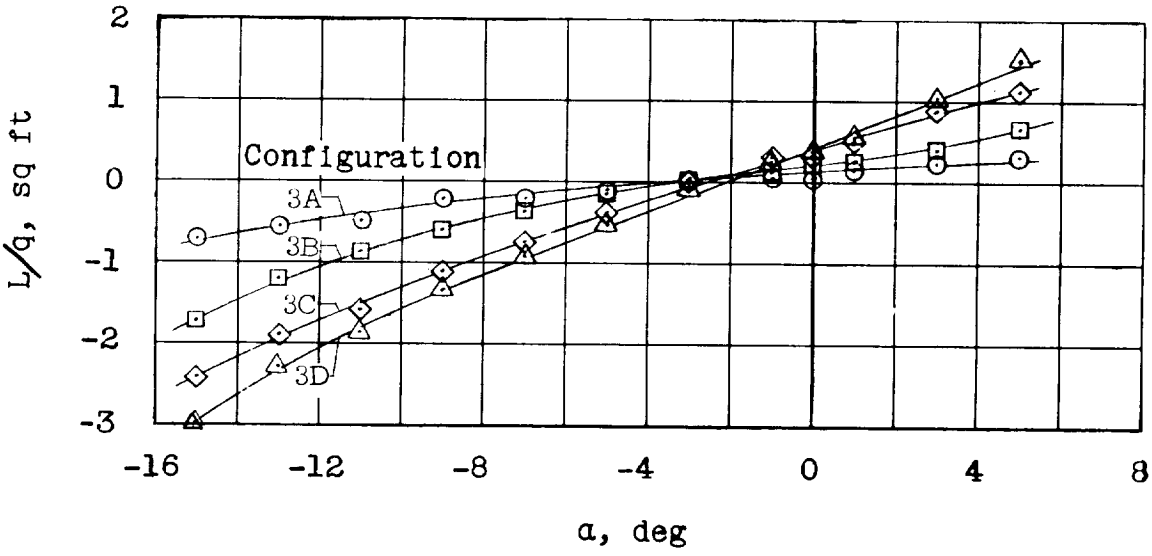

(c) Hub 3.

Figure 9.- Variation of equivalent flat-plate area representing lift with angle of attack.

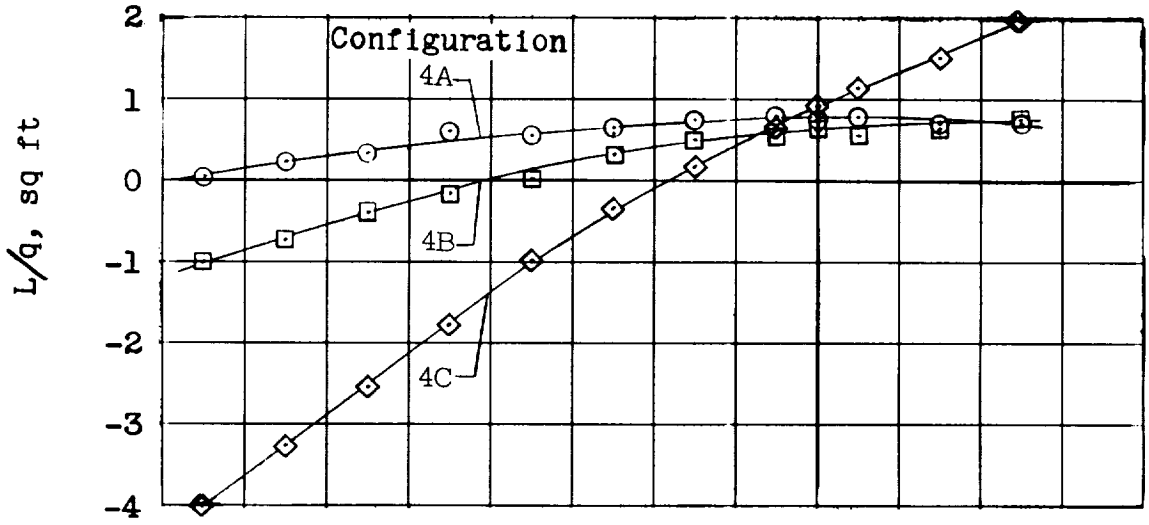

(d) Hub 4.

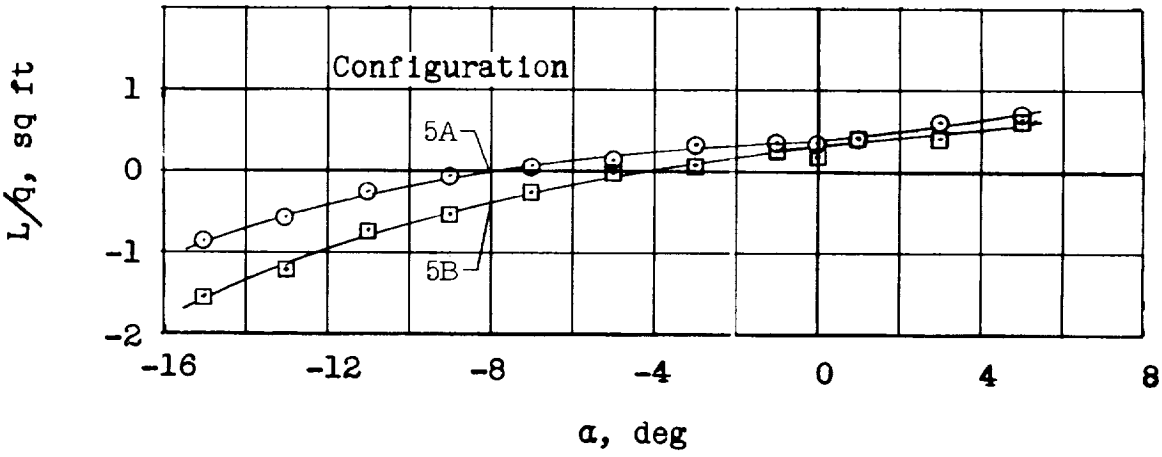

(e) Hub 5.

Figure 9.- Concluded.

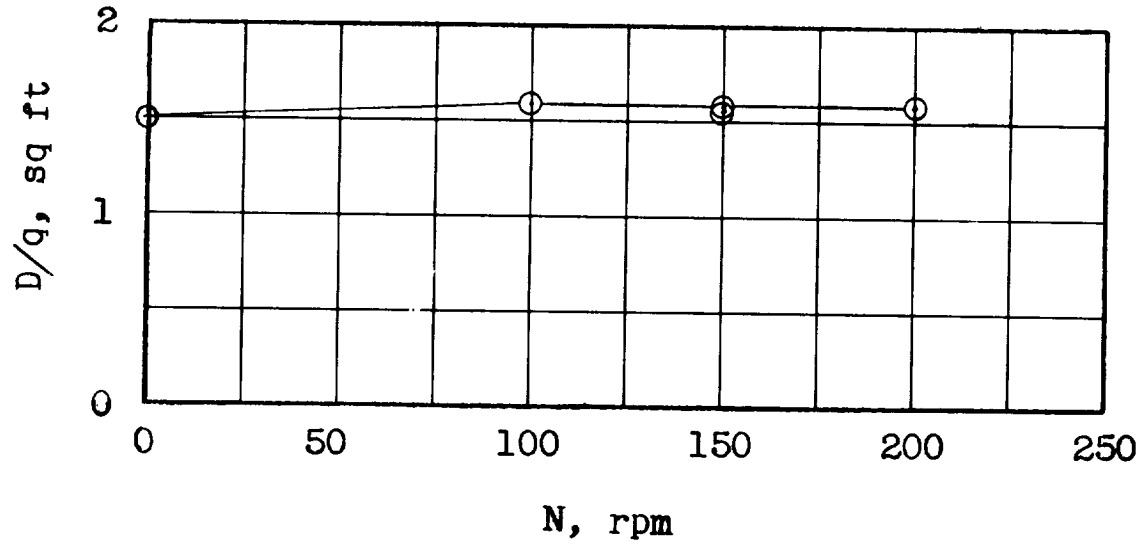

(a) Effect of rotational speed on hub 1. V = 163 ft/sec; $\alpha = 0^{\circ}$.

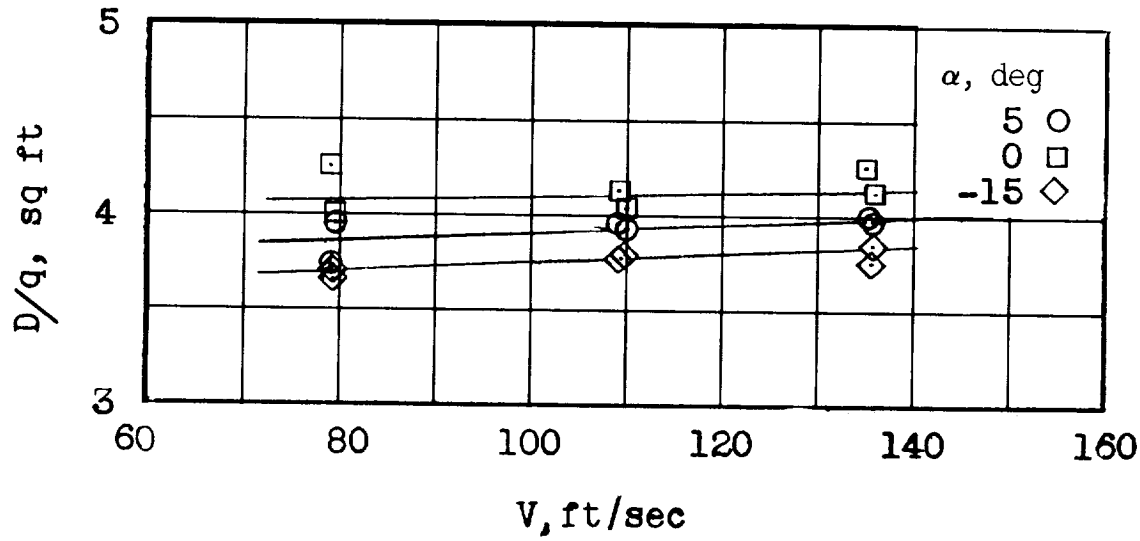

(b) Effect of forward speed on hub 4. N = 50 rpm.

Figure 10.- Effect of rotational speed and forward speed on equivalent flat-plate area representing parasite drag of hubs 1 and 4.

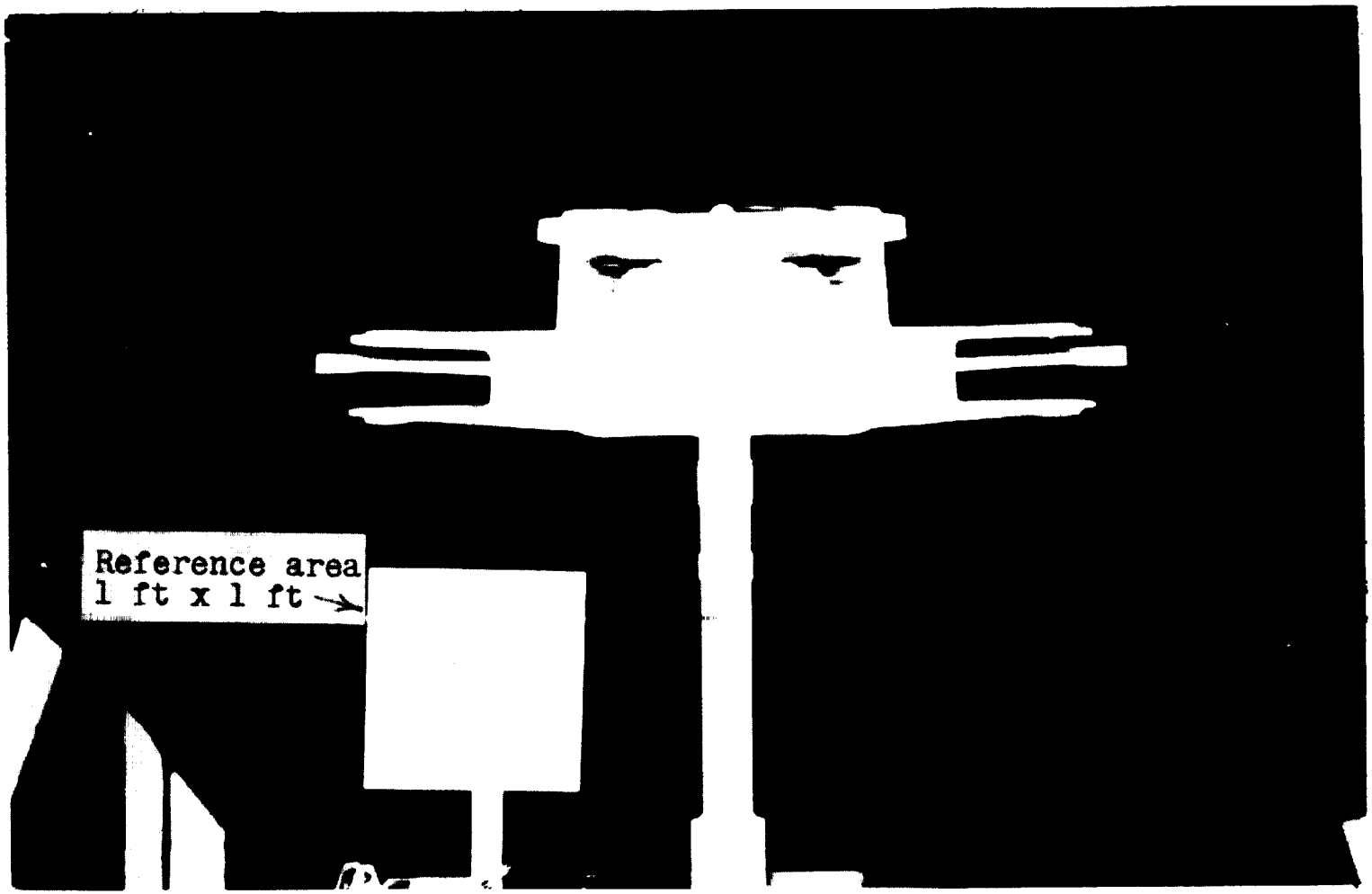

L-58-1027.1

Figure 11.- Typical time-exposure photograph used to determine projected frontal area A_p of hubs. Hub configuration 2A.

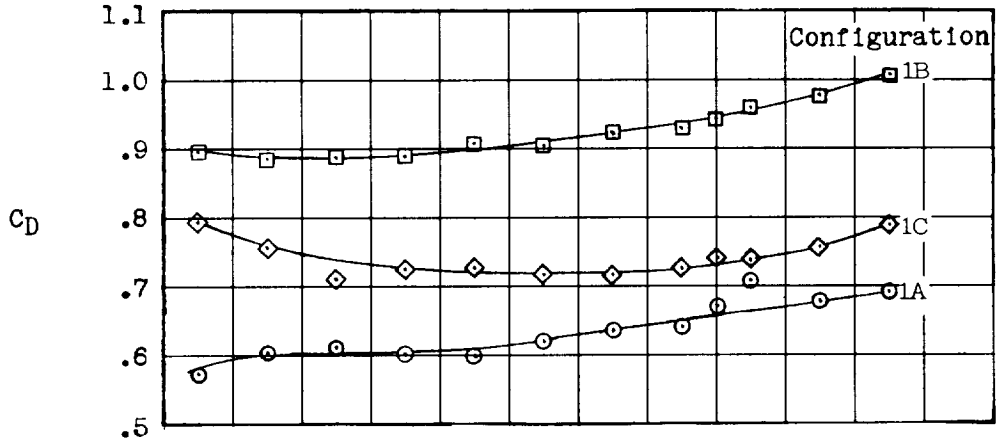

(a) Hub 1.

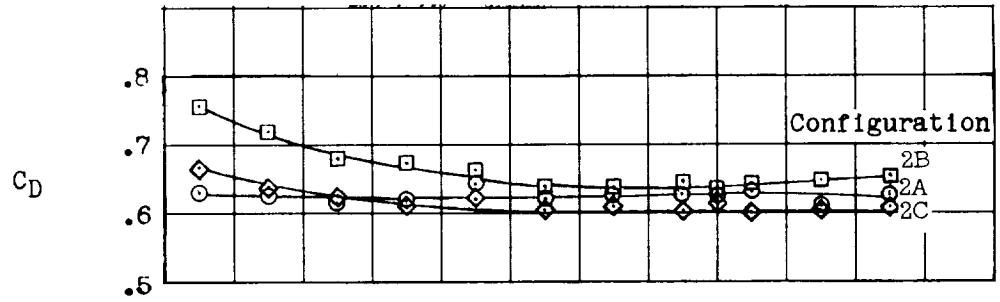

(b) Hub 2.

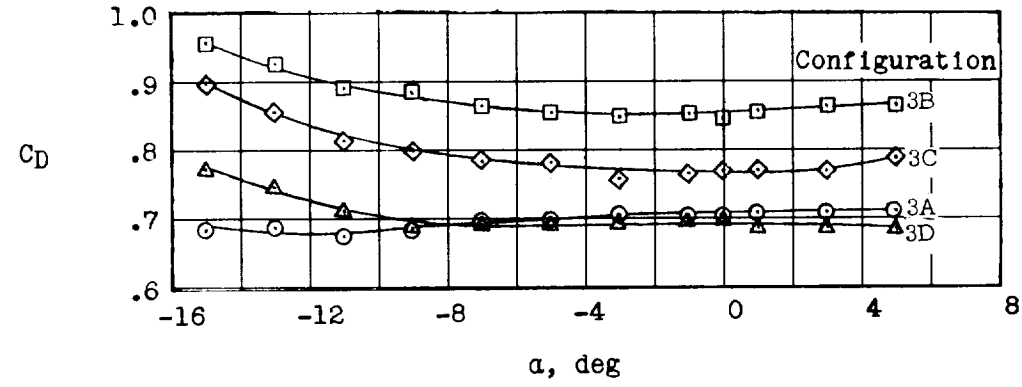

(c) Hub 3.

Figure 12.- Variation of drag coefficient with angle of attack.

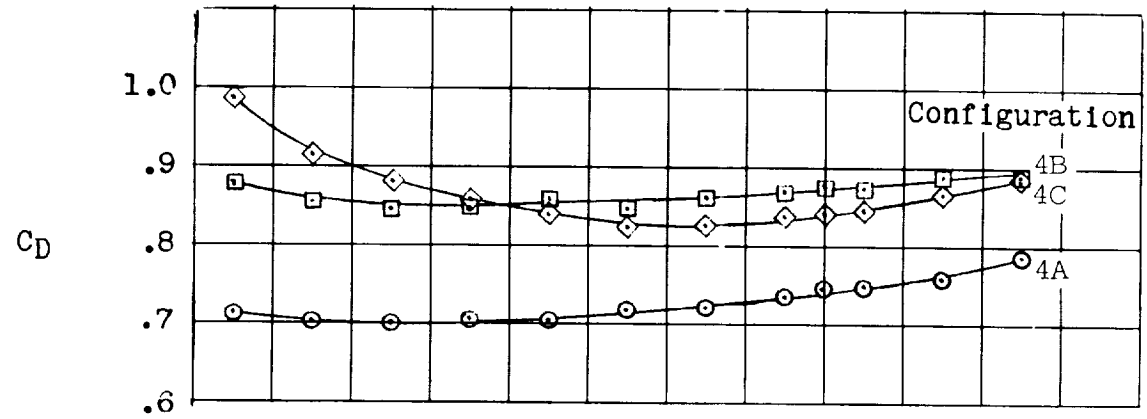

(d) Hub 4

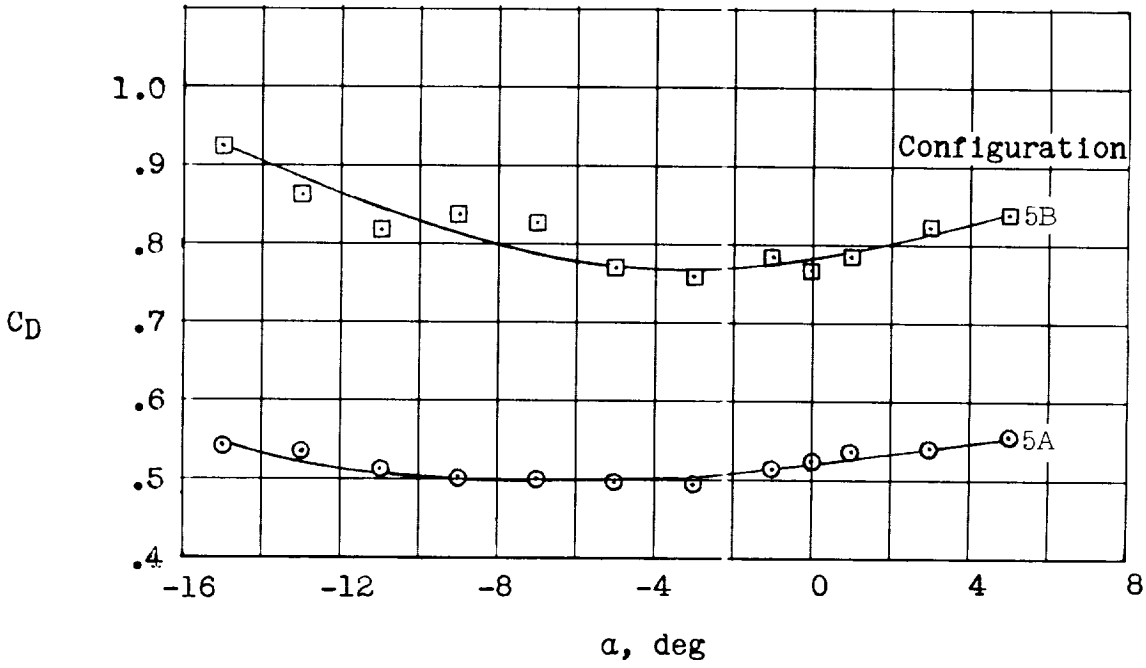

(e) Hub 5.

Figure 12.- Concluded.

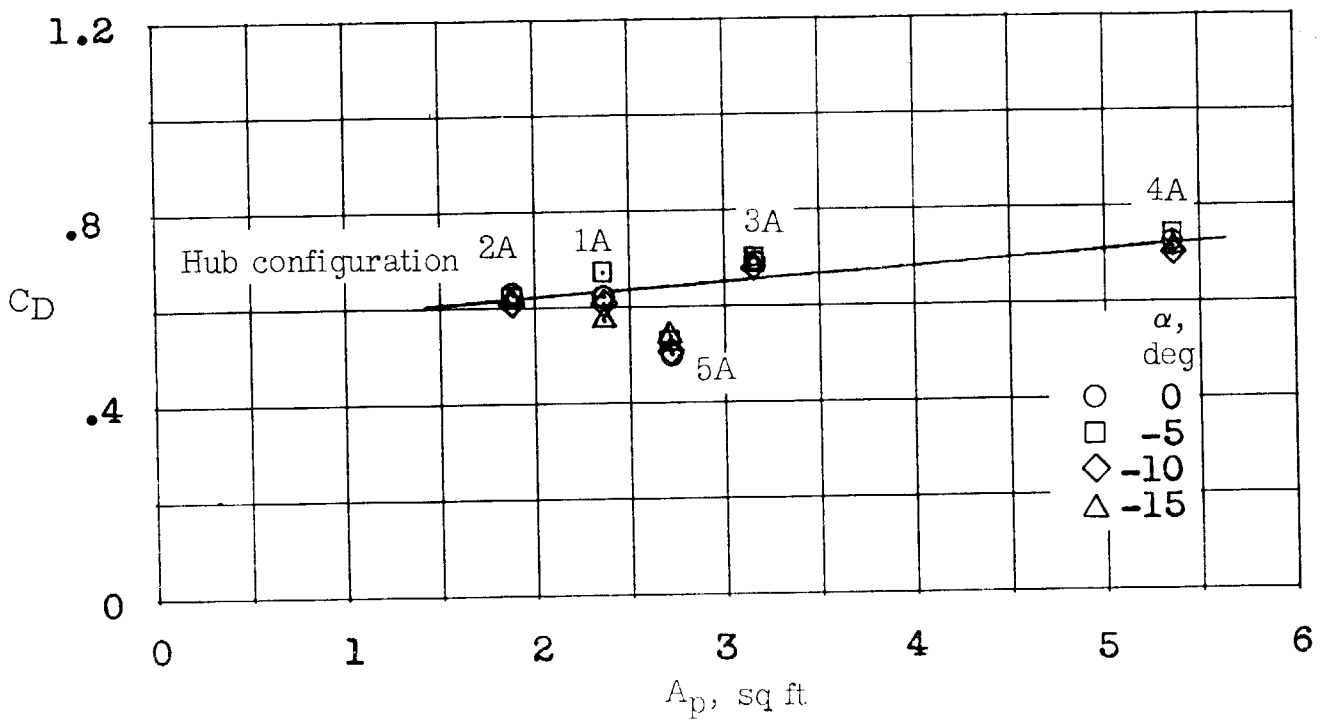

Figure 13.- Variation of drag coefficient with projected frontal area.